Appendix 1: Sampling area and studied epidote veins

The investigated epidote veins were sampled inside the Nagra Grimsel Test Site (GTS) at Grimsel Pass (Haslital), decimeters to centimeters away from Alpine shear zones (Fig. S1). The GTS is an underground rock laboratory with exposed undisturbed outcrops that are representative of the whole exhumed typical mid-crustal section exposed in the Haslital (Schneeberger et al., 2019). The veins studied here were sampled in different locations inside the GTS (Fig. S1), they are hosted by the Grimsel granodiorite (GG) and the Central Aar granite (ZAR; hereafter collectively referred to as granitoids), and they are either associated with Alpine shear zones (Fig. S2) or not. The granitoids belong to the calc-alkaline suite and their emplacement is dated at 299 ± 2 Ma for the GG and at 297 ± 2 Ma for the ZAR (Schaltegger and Corfu, 1992). The depth of intrusion is ca. 10 km (Berger et al., 2017). Both granitoids are coarse-grained and they are composed of quartz, feldspars, biotite, chlorite, white mica, epidote, titanite and other accessory minerals. The abundance of biotite in the granitoids ranges between ca. 5–15 vol. % (Wehrens et al., 2017). Epidote contents are 2 vol. % in the GG and 0.4 wt. % in the ZAR (Schneeberger et al., 2019). In the granitoids, epidote is present as both vein-filling mineral (Figs. S3 and 1C) and as feldspar alteration product (Fig. 1A), in addition to metamorphic mineral in the foliation (Fig. S3). The granitoids were involved in the Alpine orogenesis, whose deformation products are expressed by variably intense foliation and by a large number of shear zones cutting the granitoids, whose activity began at 22 Ma (Rolland et al., 2009). The shear zones developed an anastomosing network that encloses undeformed portions of the granitoids, hence highlighting a gradation from the original magmatic textures to (ultra-) mylonites (Fig. S2; Wehrens et al., 2016; 2017; Schneeberger et al., 2019). The mineralogical composition of shear zones is similar to that of the undeformed granitoids with locally higher contents of sheet silicates (Wehrens et al., 2016; Schneeberger et al., 2019). Even where the original texture of the granitoids is preserved, pervasive alteration is evidenced by saussuritization and albitization of plagioclase (Fig. 1A) and sericitization of K-feldspar, although the latter is less pervasive than the former. These feldspar alteration features are observed both in the granitoids – with feldspar grains maintaining their original habit – and in porphyroclasts in mylonites, indicating that feldspar hydration occurred at least in part before the onset of Alpine deformation. In the area, the peak conditions during Alpine deformation were estimated by Goncalves et al. (2012) at 450 ± 30 °C and 0.6 ± 0.1 kbar. A detailed characterization of granitoids and shear zones is given by Schneeberger et al. (2019; and references therein).

Epidote is here defined as minerals of the epidote–clinozoisite solid solution [$Ca_2Al_2Fe^{3+}Si_3O_{12}(OH)$–$Ca_2Al_3Si_3O_{12}(OH)$]. The occurrence of brittle epidote veins within the granitoids (Fig. S3) has been reported by Schneeberger et al. (2019; see their Fig. 4.2). The epidote veins range between decimeters to meters in length, and between ca. 1 mm to few centimeters in aperture. Their geometry is also highly variable, with some veins running rather straight and some being more sinuous. Altered feldspar and veins indicate the occurrence of fluid circulation at low temperature in the area, although the timing is unknown. A suggestion was made by Abrecht and Schaltegger (1988) that seawater infiltrated the granitoids in the Mesozoic based on whole rock (i.e., aplitic intrusions) Rb–Sr

dating indicating resetting of the isotope system, possibly in Triassic or Jurassic times. The relationship between P1 epidote vein studied here and its host rock and associated shear zone is shown in Fig. S4. Veins P2 and P3 are located ca. 1 meter away from the Alpine shear zone near which sample Grimsel-1 was collected (Fig. S2). Grimsel-2 vein is also associated with Alpine shear zones, but no field photographs or hand samples were made available. Crosscutting relationships between veins and structures of known age (e.g., shear zones, foliation) do not allow to infer an absolute timing of vein formation, which may have occurred at any time after the emplacement of the granitoids. From field relations, it is impossible to ascertain if more than one generations of epidote veins are present, and how many.

Sample P1 (Fig. S5) is an epidote-quartz ± feldspar vein with an aperture of ca. 1–5 mm in a weakly deformed portion of the Grimsel Granodiorite with sharp contacts with the host. Epidote is euhedral to subhedral and highly fractured, with grain sizes ranging between ca. 20–300 μm in size. The grain-size distribution of epidote is bimodal, with epidote grains of up to few tens of microns resulting from grain-size reduction of larger epidote relics (Fig. S5, lower panel; Fig. 2A and 2D). This indicates that the brittle process leading to the opening of the vein and to epidote mineralization was followed brittle deformation with epidote fracturing. The weak crystal zoning seen in backscattered electron (BSE) images indicates chemical zoning, whose regular pattern suggests that it results from growth processes (Fig. 2D, main text; see Franz and Liebscher, 2004), with the higher BSE contrast generally due to higher Fe and REE contents. Along with quartz (ca. 50–400 μm in size), feldspar grains of ca. 10–50 μm in size are found among epidote fragments in the smaller-sized portion of the epidote vein.

Sample P2 (Fig. S6) is hosted by a weakly deformed sector of the Central Aar Granite and it is an epidote-quartz-feldspar vein with a sharp vein–host boundary. Epidote grains measure between ca. 50 μm and 2 mm, the crystals are subhedral to anhedral with frequent pores. Quartz grains measure ca. 40–400 m, with few larger grains reaching up to 3.2 mm in length. The patterns in BSE contrast within epidote grains are locally highly irregular and cannot be entirely ascribed to growth (Fig. 2E). Likely, these BSE patterns are due to epidote recrystallization upon post-crystallization interaction with a secondary fluid. No new mineral phases resulting from the fluid-driven alteration are recognized other than epidote. Brittle fracturing of epidote grains is observed.

Sample P3 (Fig. S7) is a highly deformed epidote-quartz vein hosted by a deformed portion of the Central Aar Granite, ca. 5 mm away from an ultramylonite (Fig. S7A). The vein is locally wrapped by a foliation made of biotite and epidote (Fig. S7C), which indicates that the deformation of the vein occurred in Alpine times (Wehrens et al., 2016; 2017), and the boundary between vein and host is locally ill-defined due to such deformation. Vein epidote is subhedral to anhedral and ranges between ca. 20–150 μm in size, with the smaller grains resulting grain-size reduction of larger ones. The fracturing of epidote and the dynamic recrystallization of quartz – with single grains measuring ca. 25–200 m in size –by subgrain rotation indicate that the brittle process of vein opening was overprinted by higher-

temperature viscous deformation (e.g., Stipp et al., 2002). Regular zoning in BSE images (Fig. 2F) suggests chemical zoning related to epidote growth processes (see Franz and Liebscher, 2004).

Samples Grimsel-1 and Grimsel-2 are described in detail in Peverelli et al. (2021). The characteristics of their host rock (Central Aar granite) are the same as those of samples P2 and P3.

REFERENCES

Abrecht, J., Schaltegger, U., 1988. Aplitic intrusions in the Central Aar massif basement: geology, petrography and Rb/Sr data. Eclogae Geol. Helv. 81, 227–239. http://doi.org/10.5169/seals-166177

Berger, A., Mercolli, I., Herwegh, M., and Gnos, E.: Geological Map of the Aar Massif, Tavetsch and Gotthard Nappes, Geol. spec. Map 1:100000, explanatory notes 129, Federal Office of Topography swisstopo, Bern, Switzerland, 2017.

Peverelli, V., Ewing, T., Rubatto, D., Wille, M., Berger, A., Villa, I.M., Lanari, P., Pettke, T., Herwegh, M., 2021. U−Pb geochronology of epidote by laser ablation inductively coupled plasma mass spectrometry (LA-ICP-MS) as a tool for dating hydrothermal-vein formation. Geochronology 3, 123–147. https://doi.org/10.5194/gchron-3-123-2021

Rolland, Y., Cox, S.F., Corsini, M., 2009. Constraining deformation stages in brittle-ductile shear zones from combined field mapping and 40Ar/39Ar dating: The structural evolution of the Grimsel Pass area (Aar Massif, Swiss Alps). J. Struct. Geol. 31, 1377–1394. https://doi.org/10.1016/j.jsg.2009.08.003

Schaltegger, U., Corfu, F., 1992. The age and source of late Hercynian magmatism in the central Alps: evidence from precise U-Pb ages and initial Hf isotopes. Contrib. to Mineral. Petrol. 111, 329–344. https://doi.org/10.1007/BF00311195

Schneeberger, R.B., 2017. Interplay in 3D between faults and water flow paths in crystalline bedrock (Grimsel , Switzerland). PhD thesis.

Schneeberger, R., Kober, F., Lanyon, G.W., Mäder, U.K., Spillmann, T., Blechschmidt, I., 2019. Grimsel Test Site: Revisiting the site-specific geoscientific knowledge.

Stipp, M., Stünitz, H., Heilbronner, R., & Schmid, S. M., 2002. Dynamic recrystallization of quartz: correlation between natural and experimental conditions. Geological Society, London, Special Publications, 200(1), 171-190. https://doi.org/10.1144/GSL.SP.2001.200.01.11

Wehrens, P., Berger, A., Peters, M., Spillmann, T., Herwegh, M., 2016. Deformation at the frictional-viscous transition: Evidence for cycles of fluid-assisted embrittlement and

ductile deformation in the granitoid crust. Tectonophysics 693, 66–84. https://doi.org/10.1016/j.tecto.2016.10.022

Wehrens, P., Baumberger, R., Berger, A., Herwegh, M., 2017. How is strain localized in a meta-granitoid, mid-crustal basement section? Spatial distribution of deformation in the central Aar massif (Switzerland). J. Struct. Geol. 94, 47–67. https://doi.org/10.1016/j.jsg.2016.11.004

FIGURE CAPTIONS

FIGURE S1 Map of the Nagra Grimsel Test Site at Grimsel Pass showing the sampling locations of the studied epidote vein samples (red arrows) and the position of Alpine shear zones. Modified from Schneeberger et al. (2019).

FIGURE S2 Outcrop photograph showing the transition between undeformed texture to intense foliation in the Central Aar Granite, and the Alpine shear zone near which epidote veins P2, P3 and Grimsel-1 were sampled.

FIGURE S3 Outcrop figure showing an epidote vein and metamorphic and saussuritic epidote in the host granitoid.

FIGURE S4 Outcrop map of the sampling location of epidote vein P1 and the Alpine shear zone nearby. Mapping by Marco Herwegh.

FIGURE S5 Transmitted light microscope images of epidote vein P1. All panels are in plane-polarized light. bt = biotite; ep = epidote; fsp = feldspar; qtz = quartz.

FIGURE S6 Transmitted light microscope (A-B) and BSE (C) images of sample P2. Panel A is in plane-polarized light, panel B in cross-polarized light. Green rectangles in A show the locations of panels B and C in the thin section. bt = biotite; chl = chlorite; ep = epidote; fsp = feldspar; e-ep int. = patchy zoning resulting from fluid–epidote interaction; growth = growth zoning; qtz = quartz. White circles are laser spots (Table S1).

FIGURE S7 Transmitted light microscope images of sample P3 in plane-polarized light. Green rectangles in A indicate the locations of the microscopic images B and C, which are rotated by 90° to the right and to the left, respectively. aln = allanite; bt = biotite; ep = epidote; ep* = saussurite epidote; ep° = metamorphic epidote; fol = foliation; fsp = feldspar; qtz = quartz; ttn = titanite. Black circles indicate laser spots (Table S1).

Appendix 2: Methods

Backscattered electron (BSE) images were acquired on a Zeiss EVO50 SEM with a beam current of ca. 1 nA, accelerating voltage of 20 kV and working distance of 9.5–10.0 mm in the laboratory facilities of the University of Bern.

Epidote U–Pb isotope data were measured at University of Bern using a Resonetics RESOlutionSE 193 nm excimer laser system (Applied Spectra, USA) equipped with an S-155 large-volume constant-geometry chamber (Laurin Technic, Australia) coupled to an Agilent 7900 ICP-QMS. Tara allanite (Smye et al., 2014) was used as primary reference material with the reference isotopic values presented in Peverelli et al. (2021; their Table 2), and CAP and AVC allanite samples (Gregory et al., 2007) as secondary reference materials for quality control. Further details on the protocol can be found in Peverelli et al. (2021) and the analytical conditions used for this work are as follows:

RF power:	1400 W
Fluence:	3 J cm^{-2}
Repetition rate:	5 Hz
Cell gas flow:	3 ml min^{-1} N_2 and 400 ml min^{-1} He
Sensitivity on mass 232 in NIST612; beam size, fluence, repetition rate, scan rate:	7060 cps ppm^{-1} (samples P1 and P3)* and 6450 cps ppm^{-1} (sample P2)*; 50 µm, 2.5 J cm^{-2}, 5 Hz, 5 µm s^{-1}
232/238 ratio:	0.98
248/232 ratio:	0.002
Background:	40 s
Pre-cleaning (beam size in µm):	10 pulses (64)
Ablation time (beam size in µm):	40 s (50)
Measured masses (dwell times in ms):	206 (40), 207 (40), 208 (40), 232 (40), 238 (40)
*Samples P1 and P3 were measured on June 8th 2021, and sample P2 on June 9th 2021.	

Hydrogen isotopic measurements were carried out in ca. 4–8 mg of epidote grains at the Joint Goethe University Frankfurt–Senckenberg BiK-F Stable Isotope Facility (Frankfurt, Germany) on a Thermo high-temperature conversion elemental analyzer (TC/EA) coupled to a Thermo MAT 253 mass spectrometer in continuous flow mode. For sample preparation, epidote grains were handpicked from hand samples of veins P1–2 and Grimsel-1 under a binocular microscope and then ground in ethanol to homogenize grain sizes. Two separates of epidote P1 were made from two separate hand samples (shown in Fig. S5, upper panels) collected ca. 5 cm away from each other along the P1 vein. The resulting δD value of -77 ± 3 ‰ is the average of the values obtained from each epidote separate of -80 ± 3 ‰ and -74 ± 3 ‰, which overlap within uncertainty. Epidote separates could not be collected from sample P3 because a complete separation of epidote from biotite was not possible, and no hand specimen is available for sample Grimsel-2. Because multiphase fluid flow is inferred from epidote microstructures (Fig. 2E), H isotope analyses of feldspar hydration products – although technically feasible – are avoided as the data may represent a mixed signal between 1) fluids related to different hydration events and 2) the OH groups of epidote and mica. Effects on the measured values due to the size of the analyzed material (i.e., 4 vs. 8 mg) was ruled out in preliminary measurements of different aliquots of different grain sizes and weight of own samples (not presented here), obtaining the same δD value within uncertainty for all aliquots of each sample. Standards USGS57 (biotite), USGS58 (muscovite), NBS22

(oil) and CH7 (polyethylene foil) were analyzed for quality control, yielding δD values of, respectively, -28.4 ‰, -91.9 ‰, -100.0 ‰ and -116.9 ‰ after correction for mass bias, daily drift of the thermal combustion reactor and offset from the certified reference. An in-house standard ("epidote_1867m"; Bird et al., 1988) yielded a δD of -95 ‰. Repeated measurements of the various standards and unknowns resulted in a precision of ± 3‰ for δD. All isotope ratios are presented relative to the Vienna Standard Mean Ocean Water (V-SMOW) and $\delta D = \frac{(D/H)_{sample} - (D/H)_{reference}}{(D/H)_{reference}} \times 1000$ ‰.

We used the fractionation equation of Chacko et al. (1999) for calculation of the hydrogen isotope compositions of all epidote-forming fluids at the estimated temperatures of epidote crystallization ranging from ca. 200 to 480 °C. More in detail, the temperature of crystallization of Permian epidote of 250 ± 50 °C is estimated based on the depth of intrusion of ca. 10 km of the host rock (Berger et al., 2017). Because temperature of host rocks does not automatically translate into temperature of fluids, we have tested the effect on δD values by assuming a temperature of 600 °C (breakdown of the epidote–clinozoisite solid solution; see Franz and Liebscher, 2004) to calculate the maximum possible δD value of the Permian fluids. The fractionation factor calculated following Chacko et al. (1999) is -49.7, yielding a fluid δD of -27.3 (±3) ‰. This value is well outside uncertainty of the δD values calculated for the Alpine fluids of -14 to -10 (±3) ‰ and still consistent with a Permian fluid pathway from the surface into the granitoids exploiting syn-rift faults and interacting with syn-rift sediments. Hence, a fluid temperature of 600 °C is unlikely, and we accept the conservative estimate of 250 ± 50 °C for calculation of the δD values of the Permian fluids. It should be noted that we do not know if a normal geothermal gradient of 25 °C/km is valid for the area during Permian transtension. However, the Permian alteration cannot be high grade because of the shallow intrusion of the granite and of the basin-forming tectonics. Any uplift decreases the depth – and consequently the temperature – of the alteration, and an intrusion depth of 10 km is a conservative assumption. The large uncertainty included in these assumptions is reflected by that of ±50 °C of the estimated temperature. For Alpine epidote a temperature range of 400–600 °C is based on the breakdown temperature of the epidote–clinozoisite solid solution (Franz and Liebscher, 2004), and on the fact that the biotite is associated with epidote the veins (Peverelli et al., 2021), requiring a minimum temperature of ca. 400 °C (see Herwegh et al., 2020). The interpretation of the δD values of the epidote-forming fluids is based on a comparison with the data in Sheppard (2018; Fig. S8). A mention is necessary regarding the large δD range of meteoric waters, which is due to the dependence of H isotope fractionation with respect to topography – i.e., higher topography causes a larger extent of isotope fractionation and hence lower δD values, whereas lower-topography regions have rainwater that is closer to seawater δD values (the effect of latitude is not discussed here). Sedimentary waters refer to fluids trapped during sedimentation that equilibrate with the host sediments. Finally, the δD values of metamorphic waters are calculated from H isotopic measurements of metamorphic rocks, with metabasalts having δD values of ca. -35 to -70 ‰. Metamorphic waters extend to a δD value of 0 ‰, which is expected when seawater is released from hydrated rocks of the oceanic crust. The reader is referred to Hoefs (2018) for treatise on stable isotopes.

REFERENCES

Berger, A., Mercolli, I., Herwegh, M., and Gnos, E.: Geological Map of the Aar Massif, Tavetsch and Gotthard Nappes, Geol. spec. Map 1:100000, explanatory notes 129, Federal Office of Topography swisstopo, Bern, Switzerland, 2017.

Bird, D.K., Cho, M., Janik, C.J., Liou, J.G., Caruso, L.J., 1988. Compositional, order/disorder, and stable isotope characteristics of Al-Fe epidote, State 2-14 drill hole, Salton Sea geothermal system. J. Geophys. Res. 93, 135–144. https://doi.org/10.1029/jb093ib11p13135

Chacko, T., Riciputi, R., Cole, R., Horita, J., 1999. A new technique for determining equilibrium hydrogen isotope fractionation factors using the ion microprobe: Application to the epidote-water system. Geochim. Cosmochim. Acta 63, 1–10. https://doi.org/10.1016/S0016-7037(99)00007-1

Gregory, C.J., Rubatto, D., Allen, C.M., Williams, I.S., Hermann, J., Ireland, T., 2007. Allanite micro-geochronology: A LA-ICP-MS and SHRIMP U-Th-Pb study. Chem. Geol. 245, 162–182. https://doi.org/10.1016/j.chemgeo.2007.07.029

Herwegh, M., Berger, A., Glotzbach, C., Wangenheim, C., Mock, S., Wehrens, P., Baumberger, R., Egli, D., Kissling, E., 2020. Late stages of continent-continent collision: Timing, kinematic evolution, and exhumation of the Northern rim (Aar Massif) of the Alps. Earth-Science Rev. 200, 102959. https://doi.org/10.1016/j.earscirev.2019.102959

Hoefs, J. 2018. Stable Isotope Geochemistry. Springer International Publishing AG, part of Springer Nature 2018. https://doi.org/10.1007/978-3-319-78527-1

Peverelli, V., Ewing, T., Rubatto, D., Wille, M., Berger, A., Villa, I.M., Lanari, P., Pettke, T., Herwegh, M., 2021. U−Pb geochronology of epidote by laser ablation inductively coupled plasma mass spectrometry (LA-ICP-MS) as a tool for dating hydrothermal-vein formation. Geochronology 3, 123–147. https://doi.org/10.5194/gchron-3-123-2021

Smye, A.J., Roberts, N.M.W., Condon, D.J., Horstwood, M.S.A., Parrish, R.R., 2014. Characterising the U-Th-Pb systematics of allanite by ID and LA-ICPMS: Implications for geochronology. Geochim. Cosmochim. Acta 135, 1–28. https://doi.org/10.1016/j.gca.2014.03.021

FIGURE CAPTION

FIGURE S8 Hydrogen isotope composition of water reservoirs from Sheppard (2018) and comparison of the δD values calculated for the epidote-forming fluids investigated here. Open lines indicate that the field of possible values extends further.

Appendix 3: U–Pb isotopic data of samples P1, P2 and P3

Epidote $^{238}U/^{206}Pb$ and $^{207}Pb/^{206}Pb$ ratios are given in Table S1, whereas the Tera–Wasserburg diagrams for sample P1, P2 and P3 are presented in Fig. S9. The age uncertainties, given at 95 % confidence level, are large due to high initial Pb contents in all of the single spot analyses causing the data-points to plot close to the upper end of the regression. More in detail, in epidote (or initial Pb-rich minerals in general) U–Pb geochronology with the Tera–Wasserburg approach (Tera and Wasserburg, 1972), the age uncertainty is determined by the spread of all data-points along a regression: analyses that are rich(er) in initial Pb plot closer to the upper end of the regression. Better precision is obtained if more data-points plot away from the upper end (i.e., are initial Pb-poorer), hence constraining the lower end of the regression and consequently the age (which is given by the lower intercept between regression and concordia). For initial Pb-rich minerals, like epidote, most data-points tend to plot close to the upper end of the regression, hence large age uncertainties. This is the main limitation of epidote U–Pb dating with the Tera–Wasserburg approach, which – in turn – yields highly precise initial $^{207}Pb/^{206}Pb$ ratios. The fact that all Permian ages and Permian initial $^{207}Pb/^{206}Pb$ ratios plot within uncertainty of each other offers the advantage of being able to combine the three datasets of single samples to obtain a more precise age: by comparing the Tera–Wasserburg diagrams of single samples (Fig. S9) with Fig. 3, the effect of initial Pb-poorer analyses in bettering age precision is evident. Samples P1 and P3 were measured on June 8th 2021, with AVC and CAP allanite samples giving anchored Tera–Wasserburg ages of, respectively, 282.1 ± 3.4 Ma and 282.4 ± 4.2 Ma. On June 9th 2021, only AVC allanite was used as secondary reference material in the analytical session of sample P2, yielding an anchored Tera–Wasserburg age of 280.7 ± 4.3 Ma. All allanite Tera–Wasserburg ages are consistent with their published U–Pb ages (see Gregory et al., 2007). More details on the protocol are given in Peverelli et al. (2021).

REFERENCES

Gregory, C.J., Rubatto, D., Allen, C.M., Williams, I.S., Hermann, J., Ireland, T., 2007. Allanite micro-geochronology: A LA-ICP-MS and SHRIMP U-Th-Pb study. Chem. Geol. 245, 162–182. https://doi.org/10.1016/j.chemgeo.2007.07.029

Ludwig, K. R., 2012: User's Manual for A Geochronological Toolkit for Microsoft Excel, Berkeley Geochronology Center, Berkeley, CA, USA, 75 pp.

Peverelli, V., Ewing, T., Rubatto, D., Wille, M., Berger, A., Villa, I.M., Lanari, P., Pettke, T., Herwegh, M., 2021. U−Pb geochronology of epidote by laser ablation inductively coupled plasma mass spectrometry (LA-ICP-MS) as a tool for dating hydrothermal-vein formation. Geochronology 3, 123–147. https://doi.org/10.5194/gchron-3-123-2021

Tera, F., Wasserburg, G.J., 1972. U-Th-Pb systematics in three Apollo 14 basalts and the problem of initial Pb in lunar rocks. Earth Planet. Sci. Lett. 14, 281–304. https://doi.org/https://doi.org/10.1016/0012-821X(72)90128-8

FIGURE CAPTION

FIGURE S9 Tera–Wasserburg diagrams of samples (A) P1, (B) P2 and (C) P3. Ages are calculated from the lower intercept of the regressions through the analyses with the concordia, whereas initial 207Pb/206Pb ratios are calculated from the upper intercept of the regressions with the y axis. Dashed blue lines are regressions and dashed red lines are the error envelopes. Data-point error ellipses are 2σ, and age uncertainties are 95% confidence. The diagrams are plotted with Isoplot 3.7.5 (Ludwig, 2012).

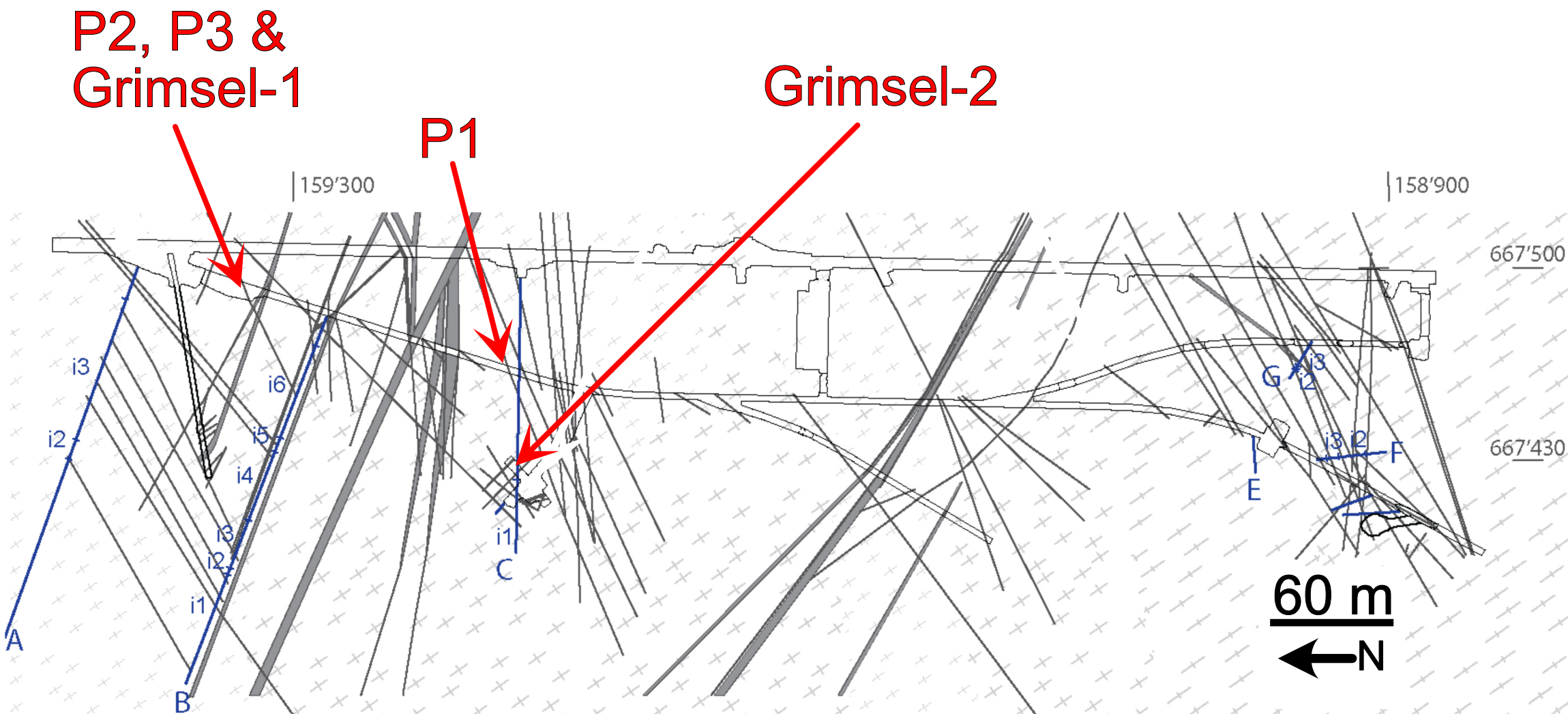

Legend

Grimsel granodiorite

Central Aar granite

Dyke

Shear zone

Borehole trace

Peverelli et al., Fig. S1, manuscript "Epidote U–Pb geochronology and H isotope geochemistry [...]"

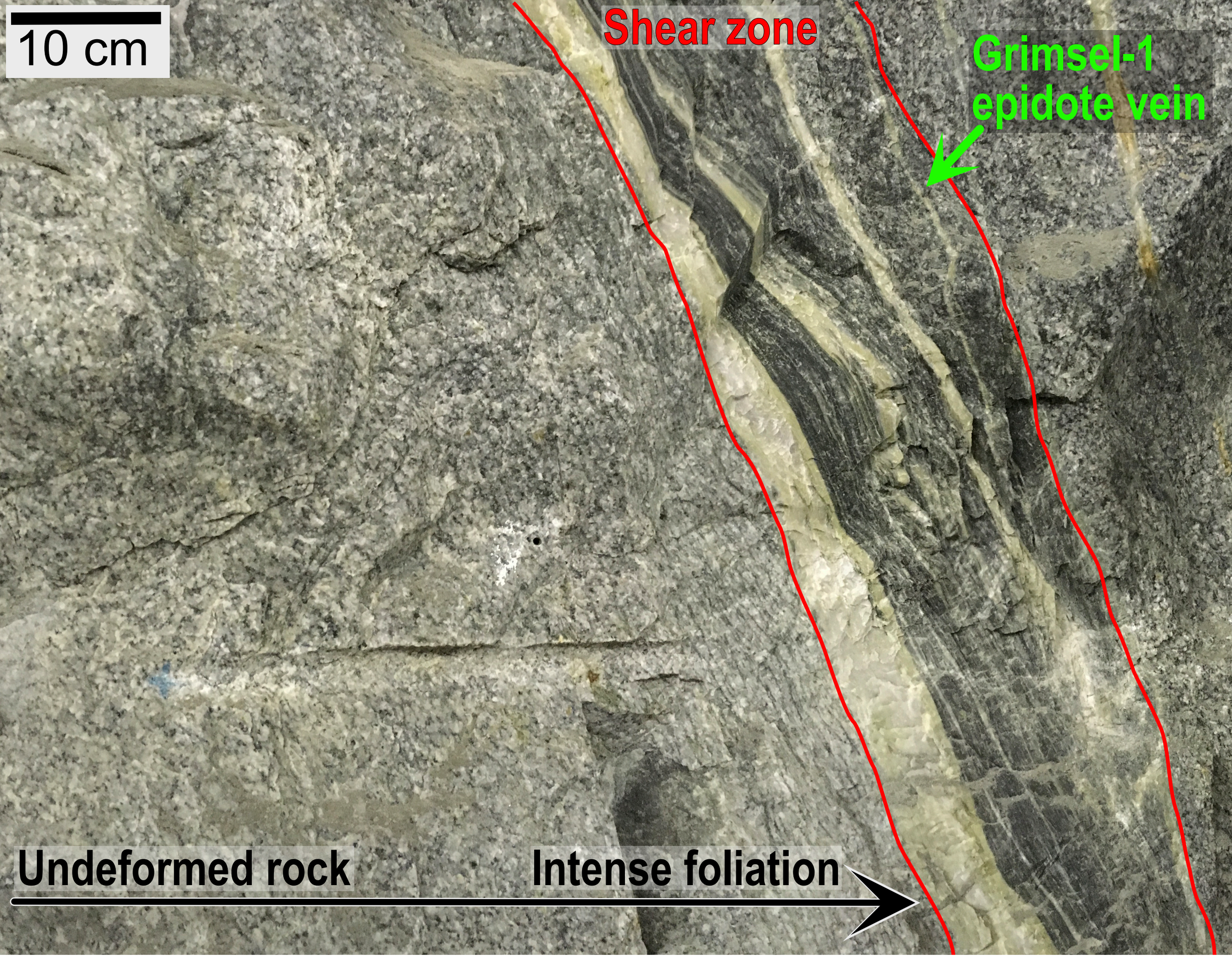

Peverelli et al., Fig. S2, manuscript "Epidote U–Pb geochronology and H isotope geochemistry [...]"

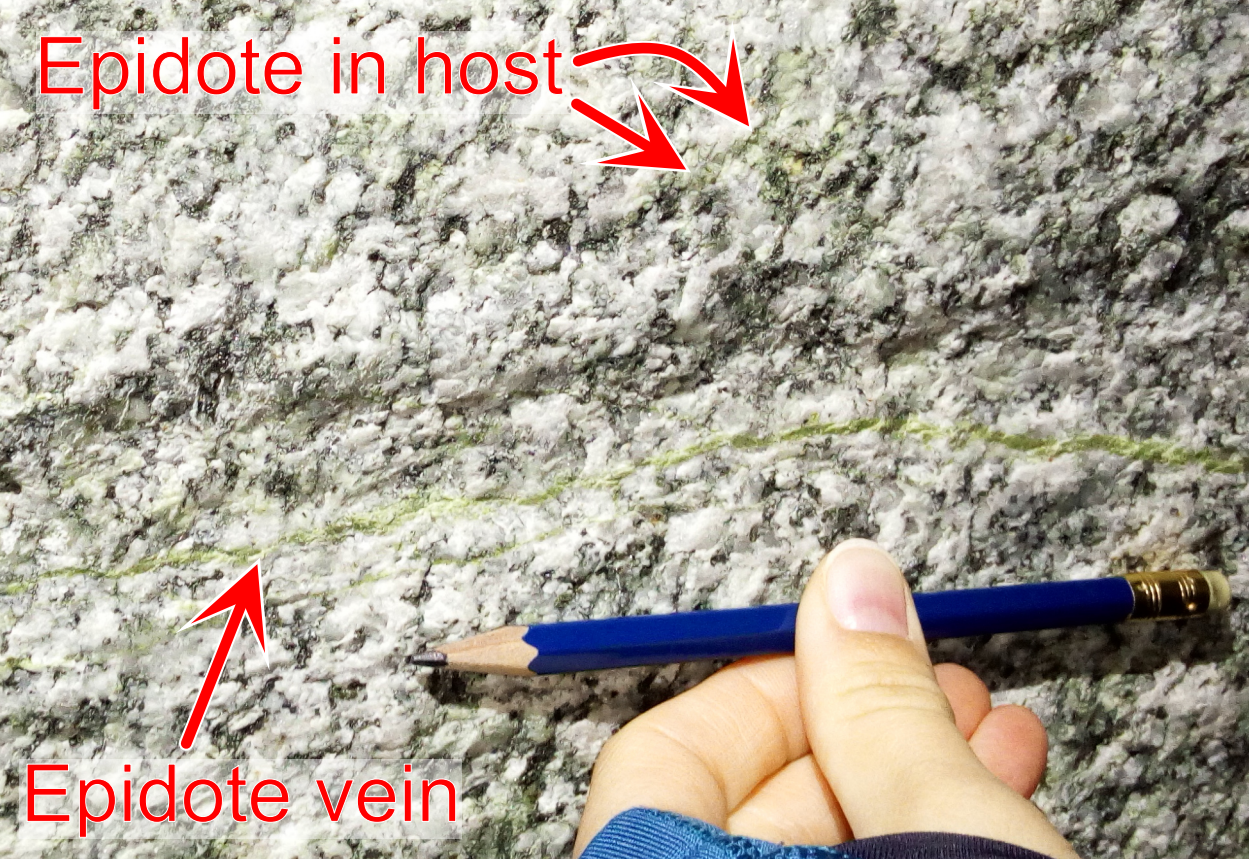

Peverelli et al., Fig. S3, manuscript "Epidote U–Pb geochronology and H isotope geochemistry [...]"

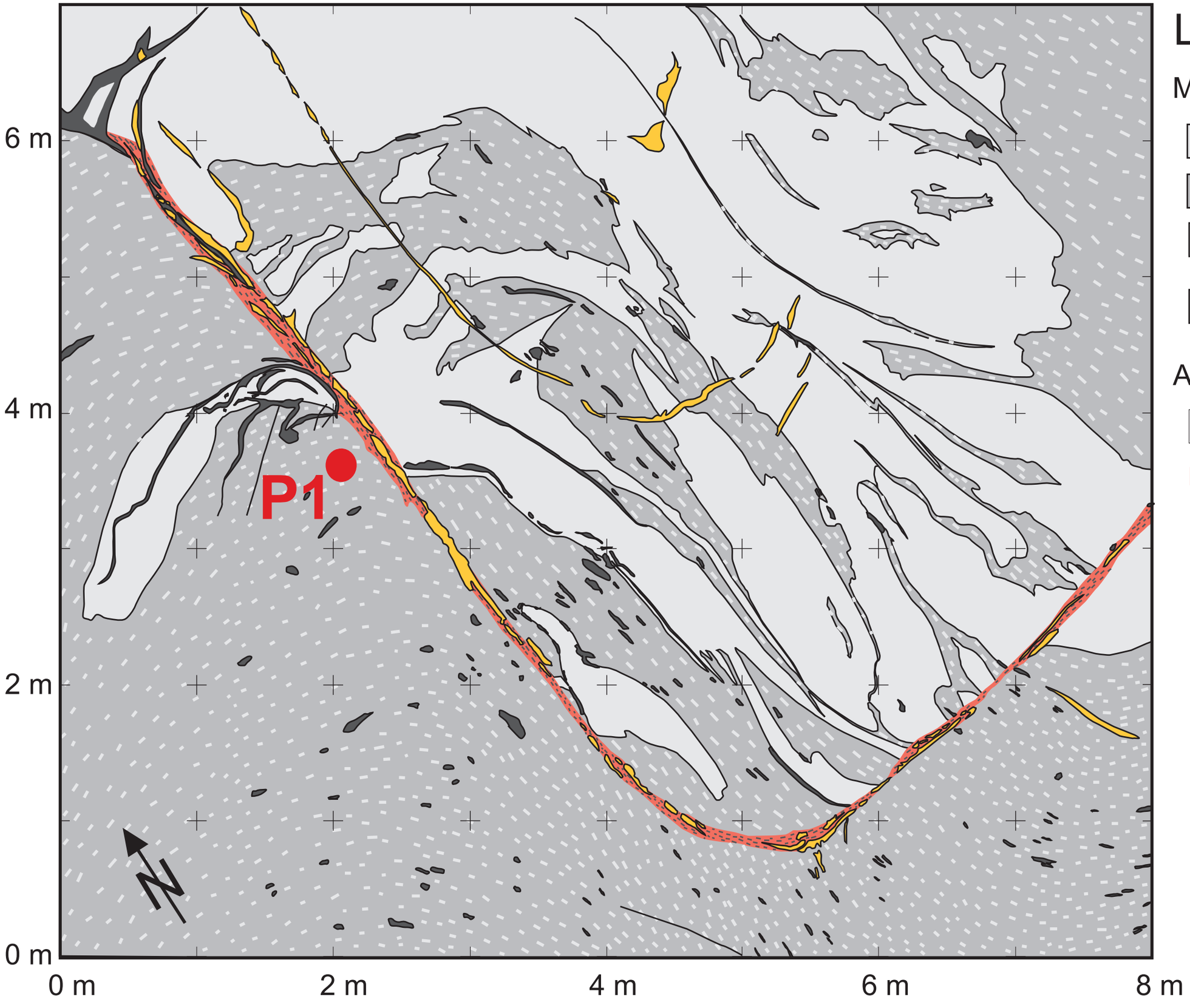

Peverelli et al., Fig. S4, manuscript "Epidote U–Pb geochronology and H isotope geochemistry [...]"

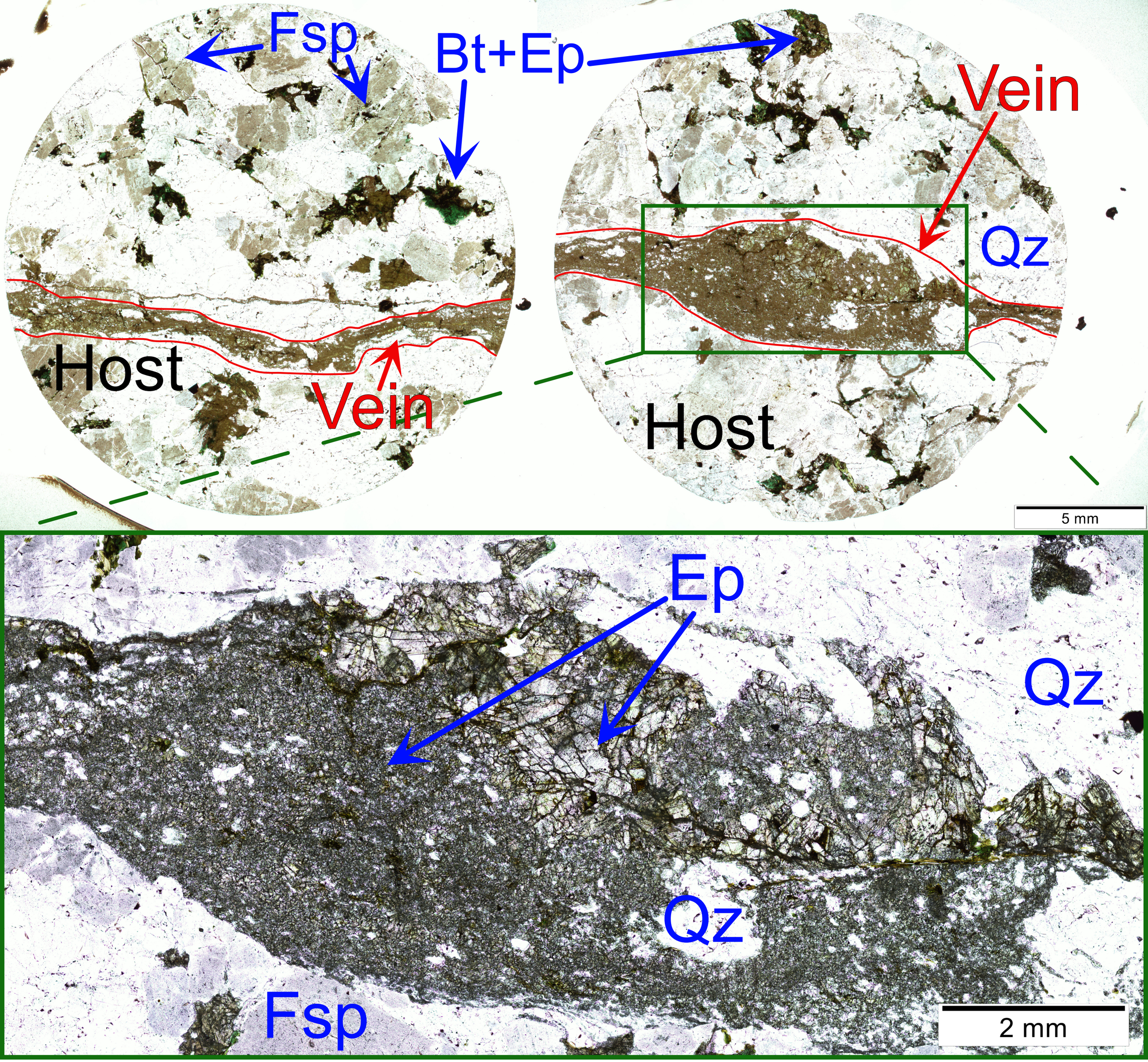

Peverelli et al., Fig. S5, manuscript "Epidote U–Pb geochronology and H isotope geochemistry [...]"

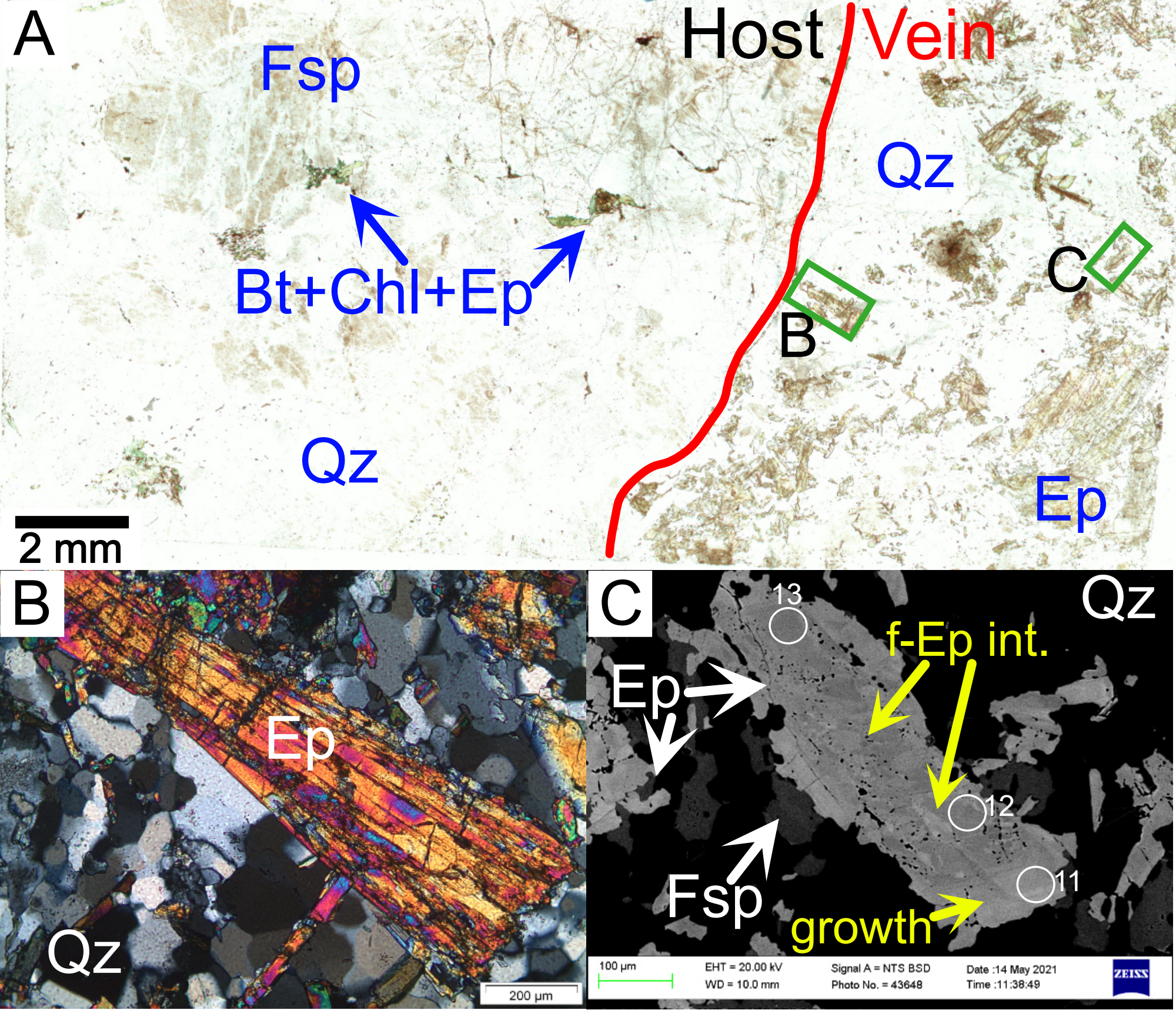

Peverelli et al., Fig. S6, manuscript "Epidote U–Pb geochronology and H isotope geochemistry [...]"

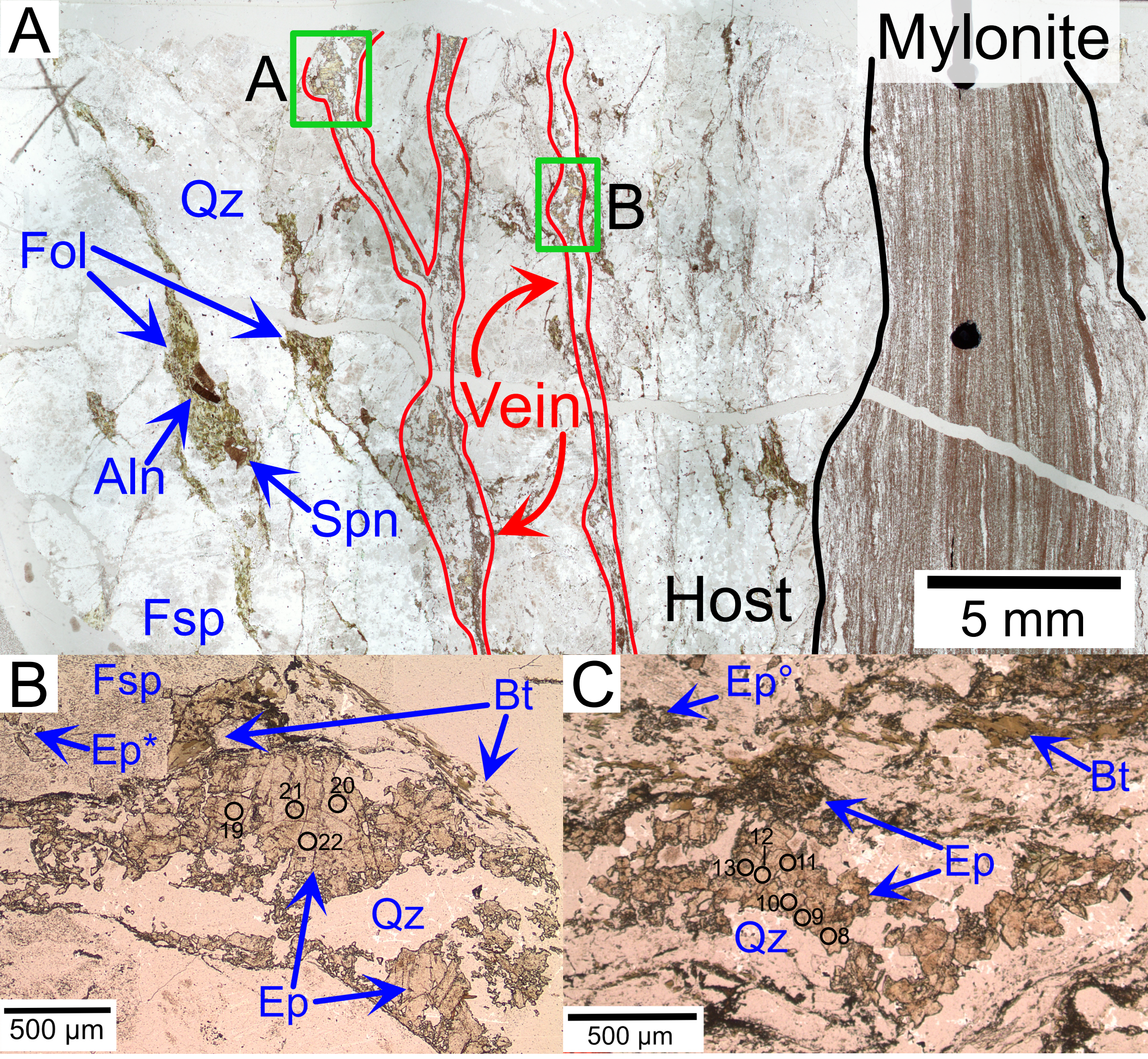

Peverelli et al., Fig. S7, manuscript "Epidote U–Pb geochronology and H isotope geochemistry [...]"

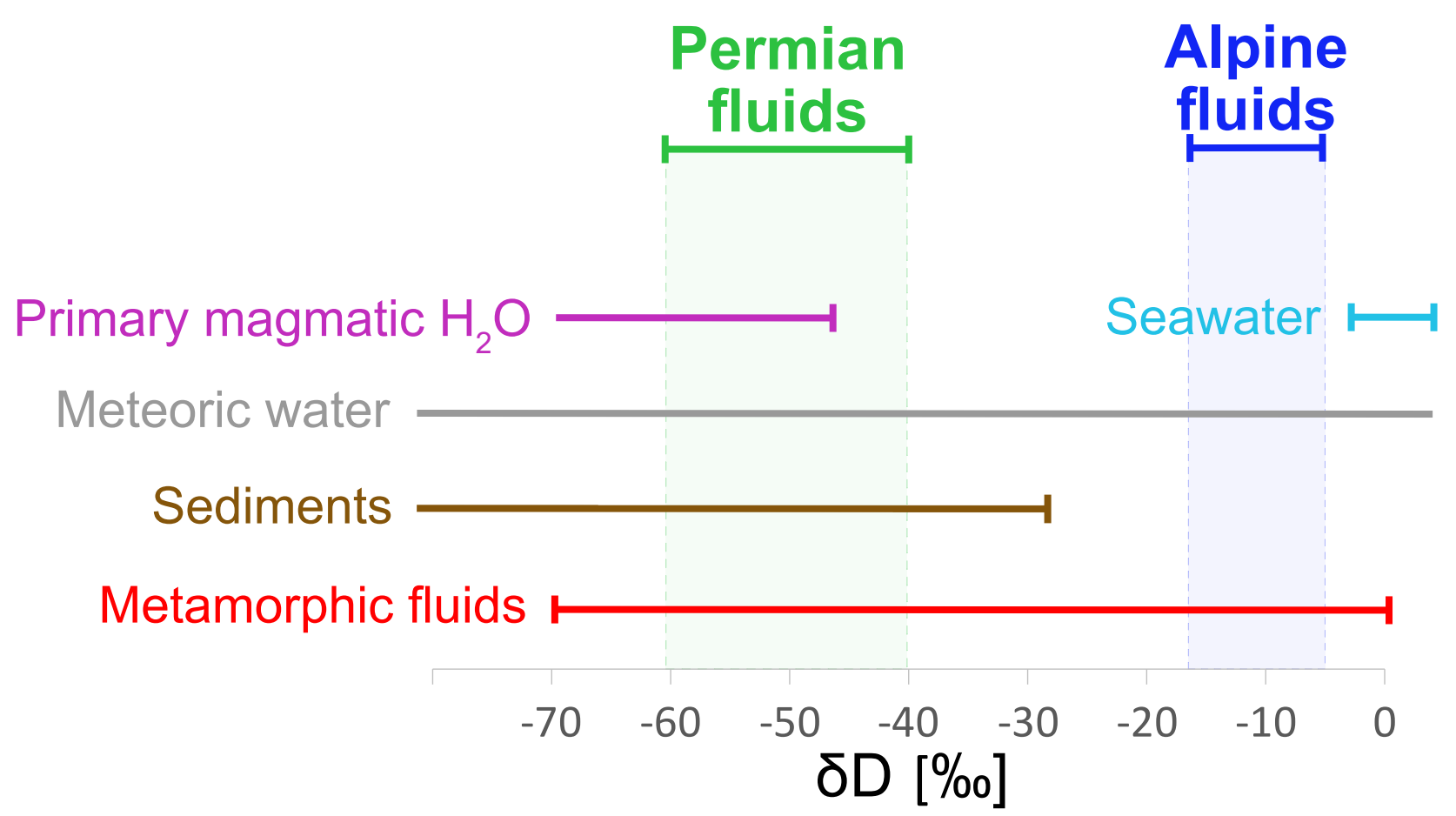

Peverelli et al., Fig. S8, manuscript "Epidote U–Pb geochronology and H isotope geochemistry [...]"

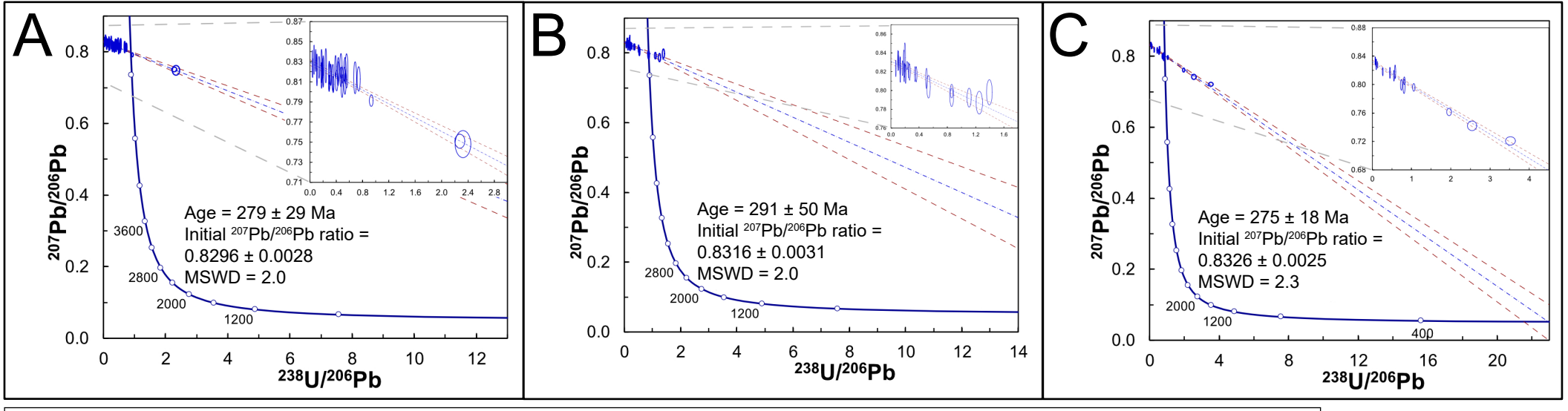

Peverelli et al., Fig. S9, manuscript "Epidote U–Pb geochronology and H isotope geochemistry [...]"